A coupled FV-SPH approach to simulate the flow around a vertical free-surface piercing cylinder

Salvatore Marrone, Andrea Colagrossi
INM INstitute of Marine engineering
CNR National Research Council
Rome, Italy
salvatore.marrone@cnr.it

Andrea Di Mascio
Industrial and Information
Engineering and Economics Dept.
University of L'Aquila
L'Aquila, Italy

David Le Touzé
LHEEA, UMR 6598, CNRS
Nantes Université, École Centrale Nantes,
Nantes, France

I. Introduction

Simulating free surface flows near rigid boundaries, whether for fundamental research or design purposes, demands numerical methods that can accurately handle the intricate evolution of the free surface—often involving significant breaking and fragmentation—while also capturing the fine details of vorticity generation in thin boundary layers along rigid walls and its subsequent development within the flow. The main challenges in producing reliable simulations for such scenarios stem from topological changes in the computational domain caused by the evolving free surface, which are more effectively addressed by Lagrangian approaches, and the need for precise resolution of the vorticity field in boundary layers and wakes, where spatial discretization is better managed using Eulerian grids.

To combine the strengths of both approaches, in [1] and [2] an algorithm that integrates the Smoothed Particle Hydrodynamics (SPH) method with a Finite Volume (FV) scheme was developed and implemented. In [3] the same approach was extended to study 3D flows. In the present work the latter algorithm is extended to the study of flow past a free-surface piercing vertical cylinder which an application typical of river hydraulics and, in particular, of the flow past bridge piers. To this purpose new features of the coupling algorithm have been implemented such as a finer control of the free-surface position and a forcing of SPH in the cylinder boundary layer.

II. Numerical method

The Navier-Stokes equations for a weakly-compressible fluid are considered. The flow domain is split in two regions: the SPH model is applied only where the free-surface deformations are relevant and the Finite Volume is utilized elsewhere. A brief description of the adopted solvers follows.

The discretization of Navier-Stokes equations in their Eulerian formulation is made by means of a Finite Volume (FV) scheme, implemented on a multi–block structured grid with partial overlapping (see [4]). A dual-time step approach is adopted to solve the discrete system of equation. The evolution of the free surface is obtained by a level-set approach: the position of the free surface is identified where the level–set function $\phi(x,t) = 0$.

The adopted SPH model is the one described in [5] in which a Primitive Variable Riemann Solver is adopted to compute fluxes between particles and a particle shifting is consistently introduced in the discrete equation system to guarantee uniform particle distributions. The latter is explicitly advanced in time through a fourth-order Runge-Kutta scheme. The kernel function adopted for the computation of the differential operators is the C2 Wendland kernel with radius equal to $R = 2.7\Delta x$, being Δx the particle size.

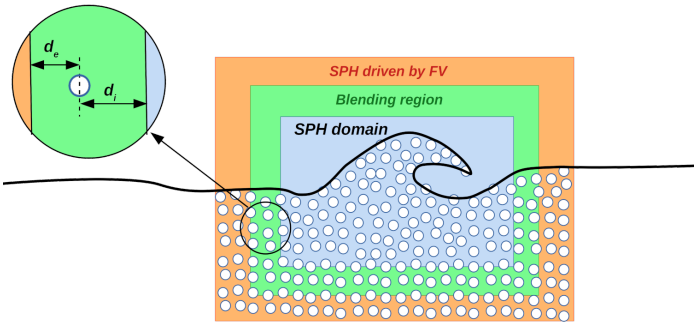

Fig. 1. Sketch of the SPH-FV domain decomposition.

III. Coupling algorithm

In order to allow information exchange, at the boundary of the SPH domain the solution from the underlying FV grid is transferred by trilinear interpolation of the values at the cell centres on a slice of SPH particles. Similarly, the solution on the FV grid is obtained by a Shepard interpolation on two slices of ghost cells.

A sketch of the adopted domain decomposition is provided in figure 1. In particular, the SPH domain consists of three separate regions: in the inner one (blue in figure 1) the solution is computed as in the standard SPH algorithm. In the intermediate region (green in figure 1), the velocity and pressure fields computed from the SPH solution are blended with the underlying FV solution with a weight that depends on the distance from the blending domain boundaries.

In the outer region (orange in figure 1) the particle motion is driven by the velocity field computed in the underlying FV solution and interpolated on the instantaneous particle positions.

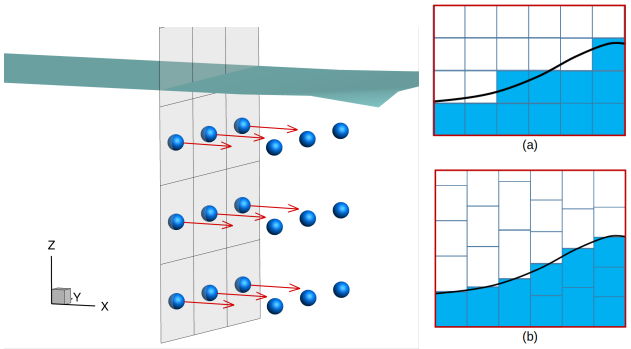

Fig. 2. Left: example of particle generated through the open boundaries. Right: representation of the free-surface across the open boundary as in [3](top) and in the present approach (bottom).

The outer boundary of the external region of the SPH domain lies in the FV domain: across this surface, particles are injected and removed on the basis of the flow direction and of the mass flow by means of the algorithm presented in [2]. Each surface of the outermost SPH domain boundary is split in sub-faces like in figure 2; from the FV solution, we integrate the mass $m_i(t)$ that flows across each face element and when $m_i(t) \geq m_0$, being $m_0 = \rho_0 \Delta x^3$, a new particle is released. When the free surface cuts across the open boundaries only immersed face elements are allowed to integrate the mass flux. In [3] this was achieved by switching on (or off) face elements whose barycenter lays below (or above) the free surface (see inset (a) in figure 2). In this way the free-surface roughly described as a step function on the SPH boundary.

In the present work this approach was enhanced in order to inject particles exactly at the free-surface location as resulting from FV interpolation (see inset (b) in figure 2). Face elements are stretched in a column-wise fashion (where a column represents an array of elements along the z direction, considering the z-axis as the direction perpendicular to the undisturbed free surface). If the level-set function on a face barycenter $\boldsymbol{x}_i$ is $-\Delta x < \phi(\boldsymbol{x}_i) \leq 0$ the whole column array of elements is stretched (or contracted) in order to have $\phi(\boldsymbol{x}_i) = -0.5\Delta x$ (because the free-surface is defined at a distance $0.5\Delta x$ from free-surface particles). In this way particles injected are not exactly cubic anymore. However, if there are at least 10 particles discretizing the water height in the SPH domain the resulting vertical distortion is at maximum 5% of the particle size. This possible anisotropy in the particle distribution is easily handled by the particle shifting technique which acts also in the blending region.

IV. Results

In this section the coupling algorithm described above is applied to the problem of the flow past a free-surface piercing vertical cylinder. To this purpose the experimental campaign described in [6] is considered: a circular cylinder of diameter $D = 0.04m$ is vertically mounted in the middle of a flume which is $10D$ wide and $100D$ long. In the present study the test case characterized by zero slope and discharge $Q = 10l/s$ is considered. The water elevation at the inlet is $H = 1.4D$ and the resulting Froude number is $\text{Fr} = U/\sqrt{gH} = 0.713$; the Reynolds number referred to the cylinder diameter is $\text{Re} = UD/\nu = 17,840$. Given the low water elevation with respect to the cylinder diameter a strong influence of bottom wall is expected on the flow. Thus, boundary layers shall be accurately resolved on both the cylinder wall and the underlying bottom wall.

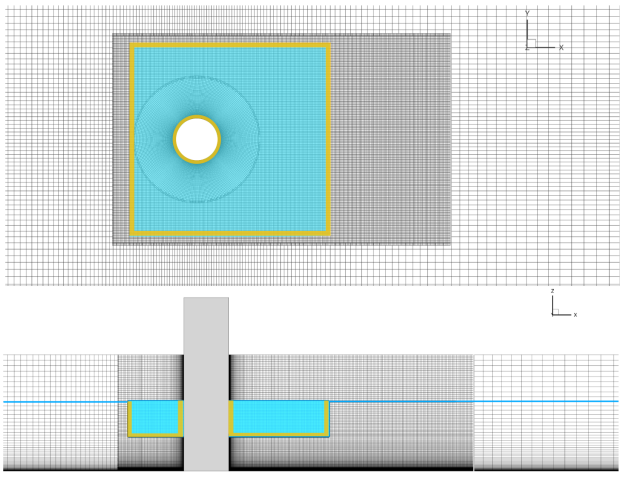

Fig. 3. Numerical domains (SPH in blue) adopted.

A. Numerical domain

In the top plot of figure 3 a portion of the FV grid in the xy-plane is depicted. Clustering of grid points is applied along the cylinder walls through the use of a circular mesh stretched in the radial direction. Then, two rectangular mesh are used: a finer one to resolve the wake up to a distance equal to 6D from the cylinder center and a coarser one for the far field.

In the same figure the overlying SPH domain (in blue) is reported along with the buffer regions (in yellow). The SPH domain covers only a portion of the water depth as the part close to the bottom is resolved by the FV through the use of suitably clustered mesh points. From the top plot of figure 3 it is possible to note a yellow strip around the cylinder. It indicates that in a annulus around the cylinder with thickness equal to the kernel radius the particles are forced with the FV solution. This is done in order to keep the FV accuracy in the resolution of the cylinder boundary layer. However, in this region particles are not generated nor deleted but only advected according to the FV solution.

B. Flow evolution

In Figure 4, an overview of the free surface flow at $tU/D = 60$ is presented. The colours indicate the horizontal velocity component. The flow striking the cylinder causes the free surface to rise, forming a horse-shoe-shaped wave in front of the cylinder. This wave is interrupted downstream by a hydraulic jump, which results from the interaction between the accelerated

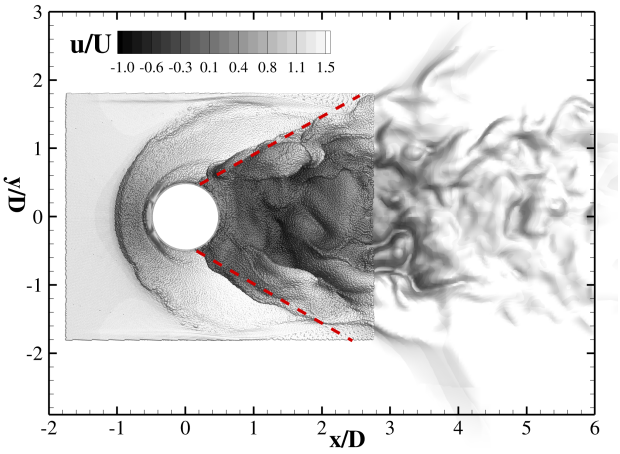

Fig. 4. Top viev of the computed free surface. The free surface is depicted through particles in the SPH region and iso-surfaces at $\phi = 0$ in the FV region. Red dashed lines represent the hydraulic jump boundaries as observed in [6].

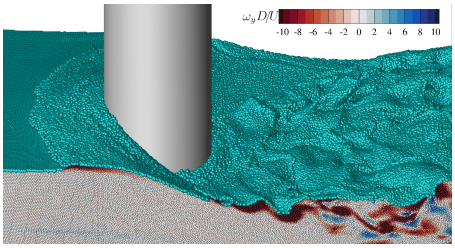

Fig. 5. Contour of the y-component of the vorticity field on the plane $y/D = -1$.

stream flowing around the cylinder and the recirculating flow behind it.

A roller generated by this process is clearly visible in the SPH region as a distinct scar on the free surface, marking two regions of the flow with different velocities (see also Figure 5). The red dashed lines highlight the boundaries of the hydraulic jump, consistent with observations from [6].

Further comparison with experimental data is shown in Figure 6, where the water elevation along the midline, as measured in the experiments, is compared to the results obtained from the coupled SPH-FV solution. Both the surge of water in front of the cylinder and the depression behind it are accurately captured.

Finally, in Figure 7 the Q-criterion is used to visualize the vortex structures generated in the flow. A characteristic horse-shoe vortex is clearly observed at the base of the cylinder. Additionally, pairs of vortex structures perpendicular to the cylinder appear in the rear-upper region of the cylinder. These vortices are generated by the hydraulic jump and subsequently travel along the wake, interacting with the vorticity shed by the cylinder.

V. Conclusions

A SPH-FV coupling algorithm has been presented and applied to the flow past a free-surface piercing vertical cylinder. New features of the coupling algorithm include a more precise

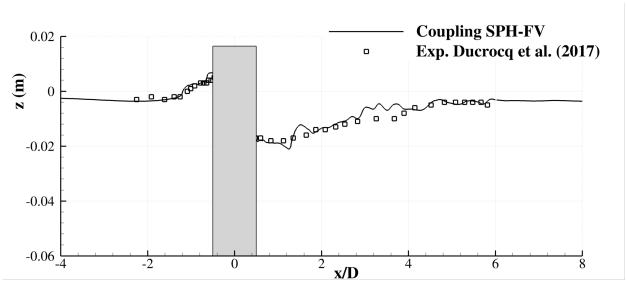

Fig. 6. Comparison of the free-surface elevation between the present results and experimental data in [6].

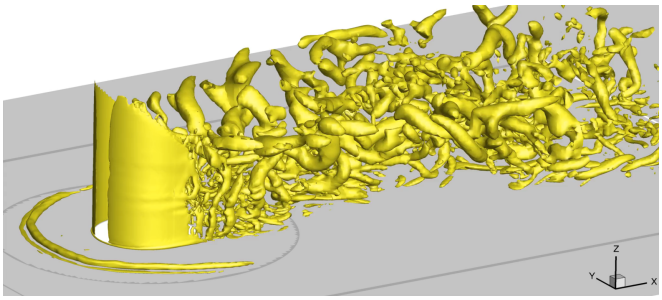

Fig. 7. Iso-surface obtained though Q criterion (Q=10).

description of the free surface at the open boundaries and addional forcing regions close to the wall boundary layers. These extensions allowed the accurate simulation of boundary layer features of the flow as well as the complex free-surface evolution behind the cylinder.

Acknowledgments

The work was supported by the project "Next Generation SPH schemes for complex multiphase flows" NEOGEO (CUP B83C23003850006) in collaboration with Ecole Centrale de Nantes in the framework of their Chair programme funded by Siemens Digital Industries Software. The work was also partially supported by the Project BIO-EMBRACE, PRIN PNRR P202298P25 - CUP B53D23026860001, financed by the European Union – Next Generation EU.

References

[1] S. Marrone, A. D. Mascio, and D. L. Touzé, "Coupling of Smoothed Particle Hydrodynamics with Finite Volume method for free-surface flows," *Journal of Computational Physics*, vol. Available online 11 December 2015, pp. –, 2016.

[2] L. Chiron, S. Marrone, A. Di Mascio, and D. Le Touzé, "Coupled sph–fv method with net vorticity and mass transfer," *Journal of Computational Physics*, vol. 364, pp. 111–136, 2018.

[3] A. Di Mascio, S. Marrone, A. Colagrossi, L. Chiron, and D. Le Touzé, "Sph–fv coupling algorithm for solving multi-scale three-dimensional free-surface flows," *Applied Ocean Research*, vol. 115, p. 102846, 2021.

[4] A. Di Mascio, R. Muscari, and G. Dubbioso, "On the wake dynamics of a propeller operating in drift," *Journal of fluid mechanics*, vol. 754, pp. 263–307, 2014.

[5] J. Michel, M. Antuono, G. Oger, and S. Marrone, "Energy balance in quasi-lagrangian riemann-based sph schemes," *Computer Methods in Applied Mechanics and Engineering*, vol. 410, p. 116015, 2023.

[6] T. Ducrocq, L. Cassan, J. Chorda, and H. Roux, "Flow and drag force around a free surface piercing cylinder for environmental applications," *Environmental Fluid Mechanics*, vol. 17, no. 4, pp. 629–645, 2017.